JOURNAL OF GEOPHYSICAL RESEARCH, VOL. 105, NO. E8, PAGES 20,281–20,295, AUGUST 25, 2000

Photometric properties of the lunar surface derived from Clementine observations

M. A. Kreslavsky, Yu. G. Shkuratov, Yu. I. Velikodsky,
V. G. Kaydash, and D. G. Stankevich

Astronomical Observatory of Kharkov State University, Kharkov, Ukraine

C. M. Pieters

Department of Geological Sciences, Brown University, Providence, Rhode Island

Abstract. Photometric properties of the lunar surface in visual and near-infrared light were studied using raw images obtained with UVVIS camera during the Clementine mission. The investigation focused on several specific regions on the lunar surface, each of which was observed by Clementine at a variety of different illumination and viewing geometries. Through these observations, the dependence of the surface brightness on the observation/illumination geometry was studied. It was shown that the disk component of this dependence, that is, the variations of brightness at constant phase angle, is different for different mare areas. The color of the lunar surface also changes with changing of the observation/illumination geometry, even if under constant phase angle. The Reiner Gamma formation displays unusual photometric properties. They are consistent with the surface being smoother than the typical mare regolith surface. The UVVIS images taken at the smallest phase angles were used to study the opposition spike, that is, the sharp increase of the surface brightness near the opposition. Steepness of the phase dependence of brightness varies over a wide range for different sites.

1. Introduction

Spectrophotometric observations of the lunar surface in the visible and near-infrared ranges from both the Earth and spacecraft are widely used to estimate composition and maturity degree of the regolith. The observed brightness of the lunar surface depends on the geometry of illumination and observation. To analyze lunar reflectance spectra quantitatively, e.g., to compare them with each other and with laboratory spectra of different samples, it is necessary to bring the brightness of different lunar sites to some standard photometric conditions. This problem is critical in the analysis of Clementine image data. Variations of photometric properties from site to site place limits for accuracy needed for lunar spectral studies. On the other hand, the regional variations of the photometric properties can provide additional information about the lunar surface, primarily on its small-scale structure.

This paper is devoted to studies of the photometric properties of the lunar surface based on analysis of selected images taken by the Clementine UVVIS camera [*Nozette et al.*, 1994]. We report here results of two related studies. (1) We study the photometric function on the basis of an analysis of UVVIS images of seven study regions, each observed over a variety of illumination and viewing geometries. In this study we rely on empirical photometric models. (2) We study the opposition effect on the basis of a number of UVVIS images with the zero phase angle point. In the end of the paper we briefly consider applications of our results to problems of photometric calibration of images of the Moon and other airless bodies.

The analysis technique and new knowledge about the lunar photometric properties are the only scope of this paper. Some preliminary results and discussion of these results related to physical mechanisms and theoretical models of the lunar photometric behavior were already presented [*Kreslavsky et al.*, 1998; *Shkuratov and Kreslavsky*, 1998; *Shkuratov et al.*, 1997, 1999a; *Velikodsky et al.*, 1999].

Paper number 1999JE001150.
0148-0227/00/1999JE001150$09.00

2. Background

In this section we describe the data used and provide empirical and theoretical background to study lunar photometric properties, starting with well-known definitions and some comments.

2.1. Clementine Data Set

For the regular Clementine mapping the surface was observed approximately from the local zenith. During 2 months, almost the whole surface was covered with images. In addition to this regular mapping, Clementine took a rather large number of images in nonregular geometry, which gave us a unique opportunity to study the disk function.

UVVIS camera images were taken in the visible and near-infrared range. In this work we analyze mostly images taken with the filters A (0.41 μm), B (0.75 μm), and D (0.95 μm). We expect that the photometric characteristics of the lunar surface in the filters C (0.90 μm) and E (1.00 μm) are close to those in the filter D (0.95 μm) [*Nozette et al.*, 1994; *McEwen*, 1996].

We worked with "raw" 288 x 384 pixel sized images (Experimental Data Records) which we then corrected for electronic off-

set, dark current, frame transfer, and flat field in accordance with the procedure developed by the Brown University Clementine Team. After these calibration steps each pixel value of the image is supposed to present some quantity (measured in counts per ms) proportional to the observed surface brightness. These values were used to study the lunar photometric properties. The absolute calibration of the images was not necessary for studying the angular dependence of the photometric function. We deliberately avoid any absolute calibration of the measured brightness. All results presented below are given as ratios of the surface brightness in arbitrary units.

The calibration procedure used was somewhat different from that adopted for Clementine image processing at USGS [*McEwen et al.*, 1998]. We compared these procedures and found that the differences are minor and rarely exceed 2% of the calibrated brightness. To reduce the influence of possible inaccuracy of calibration procedure we used only images taken with gain mode 1 and offset modes 2 and 6.

Among the images taken with nonregular geometry, there are a few large series of images of the same sites taken consecutively as the spacecraft moved along its orbit. We studied brightness of the same surface areas in such series. We expect the brightness to change smoothly along each series because of changes in the observation direction. We observed some deviations of measured brightness from a smooth dependence. Noticeable "steps" in measured brightness were associated with changes of exposure duration and minor corrections of the spacecraft attitude. We analyzed the "steps" and found no systematic variations. They cannot be explained with inaccuracy of additive steps in the calibration procedure and should be considered just as random measurement errors. Thus the height of "steps" gives an estimation of relative precision of the photometric measurements with the UVVIS camera: 1.5 – 2%. Perhaps, it is impossible to obtain any reliable results with the Clementine UVVIS data set with higher precision.

The brightness values were obtained with averaging of measured data over some areas. The precision in brightness measurements of individual image pixels is often much worse because of the lossy data compression. Individual pixels brightness values are hardly applicable for any spectrophotometric study; averaging of some kind is invariably necessary.

2.2. Photometric Function and Illumination / Observation Geometry

If a surface is illuminated by a distant point light source, the scattered radiance I in some direction is proportional to the incident illuminance J:

$$I = F J . \tag{1}$$

The coefficient F is the bidirectional reflectance [e.g., *Hapke*, 1993]. If the surface is flat and isotropic, that is, all directions in the surface plane are equivalent, then F depends only on mutual orientation of the surface plane, the incidence direction, and the observation direction. This mutual orientation can be described by a set of three angles. The bidirectional reflectance as a function of these three angles is called the brightness photometric function and is referenced as just the photometric function hereafter.

The three angles describing the illumination/observation geometry in this paper are the phase angle α, photometric latitude b, and photometric longitude l. The phase angle α is the angle between the direction from the object to the light source and from the object to the observer. The plane containing the source, the object, and the observer is called scattering plane [e.g., *Hapke*, 1993]. The photometric latitude b is the angle between the normal to the surface and the scattering plane. The photometric longitude l is the angle in the scattering plane between projection of the normal and direction from the object to the observer. These angles can vary in the following ranges:

$$0 \le \alpha \le 180°, \tag{2}$$

$$-90° \le b \le 90°, \tag{3}$$

$$\alpha - 90° \le l \le 90°. \tag{4}$$

Often used also are the incidence angle i, the angle between the normal and the direction from the object to the light source, and the emergence (observation) angle ε, the angle between the normal and the direction from the object to the observer. Their ranges are

$$0 \le i \le 90°, \tag{5}$$

$$0 \le \varepsilon \le 90°, \tag{6}$$

$$|i - \varepsilon| \le \alpha \le i + \varepsilon. \tag{7}$$

The following equations relate these angles:

$$\cos i = \cos b \ \cos(\alpha - l) , \tag{8}$$

$$\cos \varepsilon = \cos b \ \cos l , \tag{9}$$

$$\tan l = \frac{\cos i / \cos \varepsilon - \cos \alpha}{\sin \alpha} , \tag{10}$$

$$\cos b = \cos \varepsilon / \cos l . \tag{11}$$

The case $l = \alpha - 90°$ corresponds to the terminator, that is, $i = 90°$. The case $l = 90°$ corresponds to the limb, that is, $\varepsilon = 90°$. The photometric function is an even function with respect to photometric latitude b: $F(\alpha, -b, l) = F(\alpha, b, l)$. The photometric function must satisfy the reciprocity principle [e.g., *Hapke*, 1993], which demands

$$F(\alpha, b, l) \cos l = F(\alpha, b, \alpha - l) \cos(\alpha - l). \tag{12}$$

2.3. Applicability of the Photometric Function

Note that the photometric function can be strictly defined only if the surface is isotropic and flat and the light source is a point. Below, we consider how we can apply these suppositions to the lunar surface.

2.3.1. Light source. We can consider each point of the solar disk as an independent point light source, which contributes to the total surface brightness but with its illumination geometry slightly different from other points of the solar disk. The resulting brightness of the surface can be obtained as a convolution of the "point-source" photometric function with a properly transformed distribution of brightness over the solar disk. Obtained in this way the "real-Sun" photometric function will be equal to the "point-source" photometric function for the center of the solar disk with great accuracy, when the phase angle α is much greater than the angular size of the Sun (0.5°). For small phase angles one cannot equate the observed photometric function with the "point-source" one [*Shkuratov*, 1991; *Shkuratov and Stankevich*, 1995].

2.3.2. Surface isotropy. If there are peculiar directions in the scattering surface, the bidirectional reflectance is not a function of three angles: one more angle is necessary.

The assumption of lunar surface isotropy is based primarily on common sense. Photometric behavior is controlled primarily by subcentimeter-scale structure of the regolith. This structure is formed owing largely to micrometeorite bombardment. No obvious reason is known for the production of any anisotropy in this process. Cosmic rays and solar wind could also influence photometric properties through the submillimeter and smaller structure. Solar wind treats the lunar surface anisotropically and could cause minor anisotropy of photometric properties of mature regolith, especially at high latitudes. However, such anisotropy cannot be directly revealed in photometric observations, if the Sun is used as a light source.

To check the isotropy, one needs to compare surface brightness of the same site under the same photometric latitude, longitude, and phase angle, but for different Sun azimuths. For the Earth-based observations such comparison is impossible. The set of Clementine UVVIS images gives a little possibility for such a direct test. During the regular mapping a narrow (about 20-30 pixels wide) strip on the farside was imaged twice from local zenith (that is, with $b \approx l \approx 0$) with exactly the same incidence angles (and hence the same phase angles), but with different Sun azimuths. We coregistered these images and obtained images of brightness difference. These difference images obviously revealed local topography. For a few rather smooth sites we saw some faint (just-above-noise) gradual variations in these images. We cannot rule out that they are due to variations of anisotropy, but we also cannot rule out a number of other explanations.

2.3.3. Flatness. When estimating local angles of incidence and emergence for any point of the Moon, it is often routinely assumed that the surface is flat. However, the lunar surface is not flat, and topography can vary considerably with size scale. The topographic features range from the planetary scale (greatest basins) to the regolith microrelief.

Topography at the scale that is much larger than the spatial resolution can be treated as local variation the of observation/illumination geometry due to surface tilt. Surface tilt that can be ignored at given accuracy is steeper for small phase angles. Resolution-scale topographic features cannot be treated in this way, and photometric study of them with the images of given resolution is impossible. Topography on the scale much smaller than the observation resolution affects the photometric behavior through the average brightness contributed by many variously tilted unresolved surface elements. The higher the resolution, the steeper the typical surface tilts [e.g., *Sayles and Thomas*, 1978]. This means that the photometric function can depend on spatial resolution. Hence a special consideration is necessary when comparing, for example, the lunar photometric function derived from Earth-based data with Clementine observations of the Moon or with laboratory studies.

Problems related to the resolution-scale surface topography are most evident for oblique illumination and/or viewing. Photometric function can practically be used if angular heights of the light source $90°-i$ and the observer $90°-\varepsilon$ are greater than a typical surface tilt at the scale of the observation resolution. This limit depends on resolution. The higher the resolution, the steeper the typical surface tilts, hence the narrower the range of illumination / observation geometry where the photometric function can be applied.

2.4. Phase Function and Disk Function

In this study it is convenient to present the photometric function $F(\alpha, b, l)$ in a factorized form:

$$F(\alpha, b, l) = A\, f(\alpha)\, D(\alpha; b, l), \tag{13}$$

where A is surface albedo at some standard observation/illumination geometry, $f(\alpha)$ is traditionally called the phase function, and $D(\alpha; b, l)$ contains all dependence of F on the photometric latitude and longitude. We will call $D(\alpha; b, l)$ the disk brightness distribution or just the disk function. Albedo A strongly varies over the lunar surface and with wavelength, while regional and spectral variations of the functions $f(\alpha)$ and $D(\alpha; b, l)$ are much smaller and often are ignored. How the dependence on α is divided between factors $f(\alpha)$ and $D(\alpha; b, l)$ in (13) is a matter of convention. In this paper we use the following standard geometry: $b = l = 0$, $\alpha = 30°$. Note that this geometry was used in laboratory spectral measurements of many lunar samples and their analogs by the Brown University RELAB facility [e.g., *Pieters*, 1998]. Thus we define

$$D(\alpha; b, l) = F(\alpha, b, l) / F(\alpha, 0, 0); \tag{14}$$

$$f(\alpha) = F(\alpha, 0, 0); \tag{15}$$

$$A = F(30°, 0, 0). \tag{16}$$

Equation (14) is a somewhat unconventional way to introduce the disk function, because due to constraint (4) it works only for $\alpha < 90°$. A more common convention is to define $D(\alpha; b, l) = F(\alpha, b, l) / F(\alpha, 0, \alpha/2)$. However, definition (14) is convenient when working with Clementine data because most of the Clementine images were taken at $b \approx l \approx 0$. In this paper we never work with phase angles higher than 90°.

Exhaustive measurements of the photometric function require filling a volume in the three-dimensional (3-D) space of parameters α, b, and l with a rather dense mesh. Clementine images do not provide such a data set for any single area on the Moon. For Earth-based observations the photometric latitude and longitude are close to the geographical latitude and longitude and vary slightly owing to libration. Hence, for each resolved point on the Moon, astronomical observations can provide information about the dependence on α but almost no information on b and l. The disk function can be studied from astronomical data if one supposes that it is the same for the entire surface (or, say, for all mare and all highlands). Studies of regional variations of the disk function from the Earth are not possible.

3. Disk Function

In this section we study problems related to brightness distribution over the lunar disk. This study is based on an analysis of UVVIS images of the same areas with different observation directions. Some preliminary results were reported by *Velikodsky et al.* [1999].

3.1. Method

For several sites the spacecraft, moving along its orbit, took a large series of images of the same area. Illumination / observation geometry changed from image to image. As a result, for these sites, we have measurements of surface brightness along some curve in the 3-D space of the angles α, b, and l. We chose the following series: orbit 299, the Apollo 15 landing site vicinity (Figure 1a); orbit 309, a site in Mare Cognitum (Figure 1b); orbit 322, the Reiner Gamma albedo feature in Oceanus Procelarum (Figure 1c); and orbit 323, a site in Oceanus Procellarum in the vicinity of the crater Galilaei (Figure 1d). The curve showing the change of b and l in the series of orbit 299 is presented in Figure

3 as an example. For the other series, such curves are similar but not the same. For the chosen sites the phase angle α initially decreases and then increases throughout the sequence of images (Figure 2). Consequently, for each α from some range we have

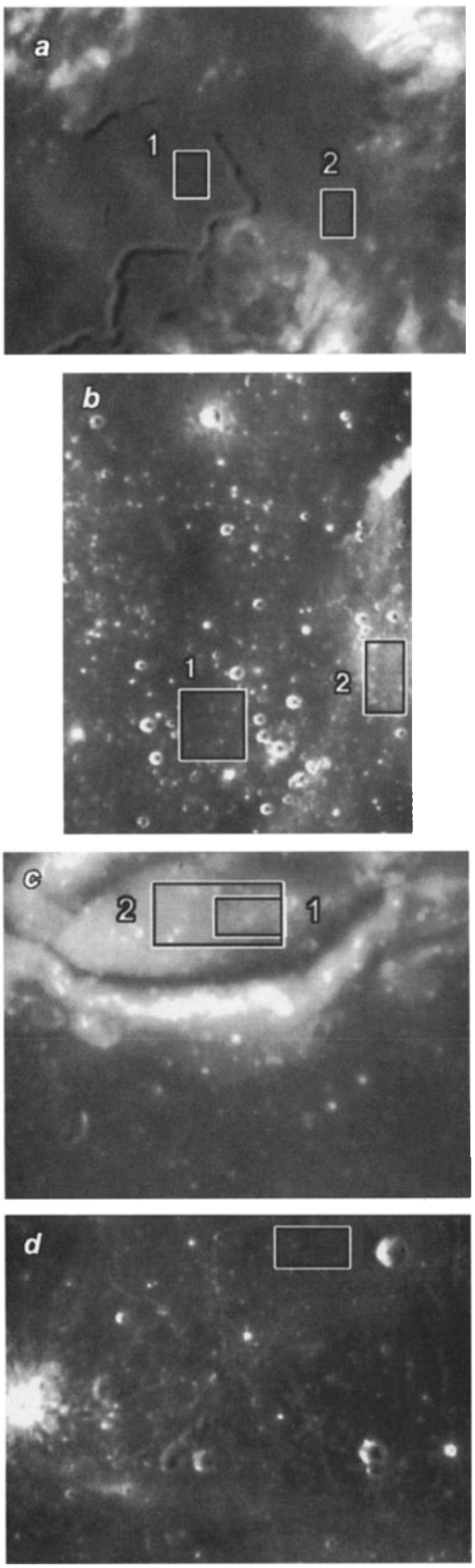

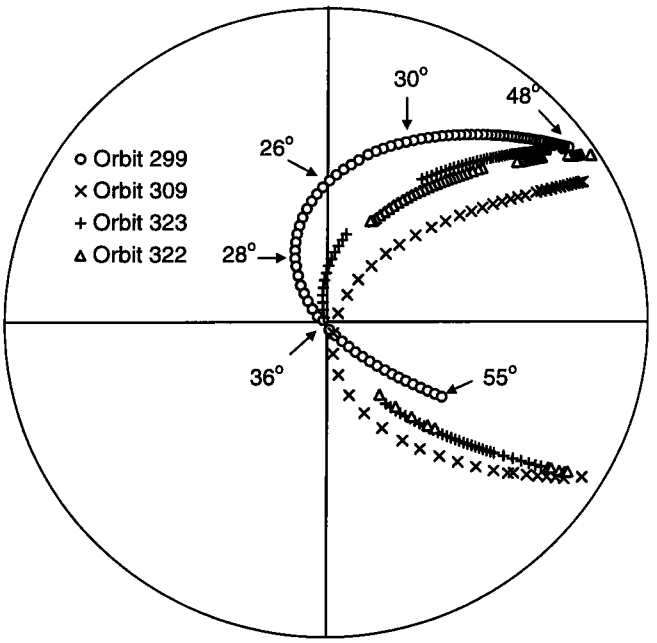

Figure 2. [TRACE.XLS->Trace] Sequences of photometric latitude and longitude in the series of images taken in orbits 299, 309, 322, and 323 for the sites shown in Figure 1. Photometric latitude and longitude are plotted in the orthographic projection. Numbers along the orbit 299 series illustrate changes of the phase angle in the series. In the other series the phase angle changes approximately in the same manner.

brightness measurements for two different sets of the angles b and l. Scale of the images changes a few times within the series, because the distance from the spacecraft to the scene changes. We assume that this change does not significantly influence the photometric function.

For each of the three sites we chose one or two rectangular areas which are as flat and homogeneous as possible. We identified these areas in each image using surface features, because the camera-positioning data did not provide sufficient accuracy. Then we averaged surface brightness in the areas for each image. As an example, the sequential measurements of the surface brightness in one of the series in the red filter are plotted against the phase angle α in Figure 3 (top curve). Two branches of the sequence demonstrate that for the same phase angles surface brightness is different owing to difference in the photometric latitude and longitude. If we divide the measured brightness by the disk function, the branches coincide. The set of four bottom curves in Figure 3 shows how different approximations of the disk function bring the branches together.

Figure 1. [a15.psd, cog.psd, fig2c.psd, l8.psd = SITES.CV5] Sites used for study of the disk function. Marked are the areas for which photometric measurements were analyzed. (a) Clementine image LUE3909L.299 of the vicinity of Apollo 15 landing site. The scene is centered at 26.2°N, 3.4°E. (b) Clementine image LUB1367I.309 of an area in Mare Cognitum. The scene is centered at 7.2°S, 23.3°W. (c) Clementine image LUB4843J.322 of Reiner Gamma. The scene is centered at 7.0°N, 59.0°W. (d) Clementine image LUB3013J.323 of an area in Oceanus Procellarum near crater Galilaei. The scene is centered at 8.7°N, 62°W.

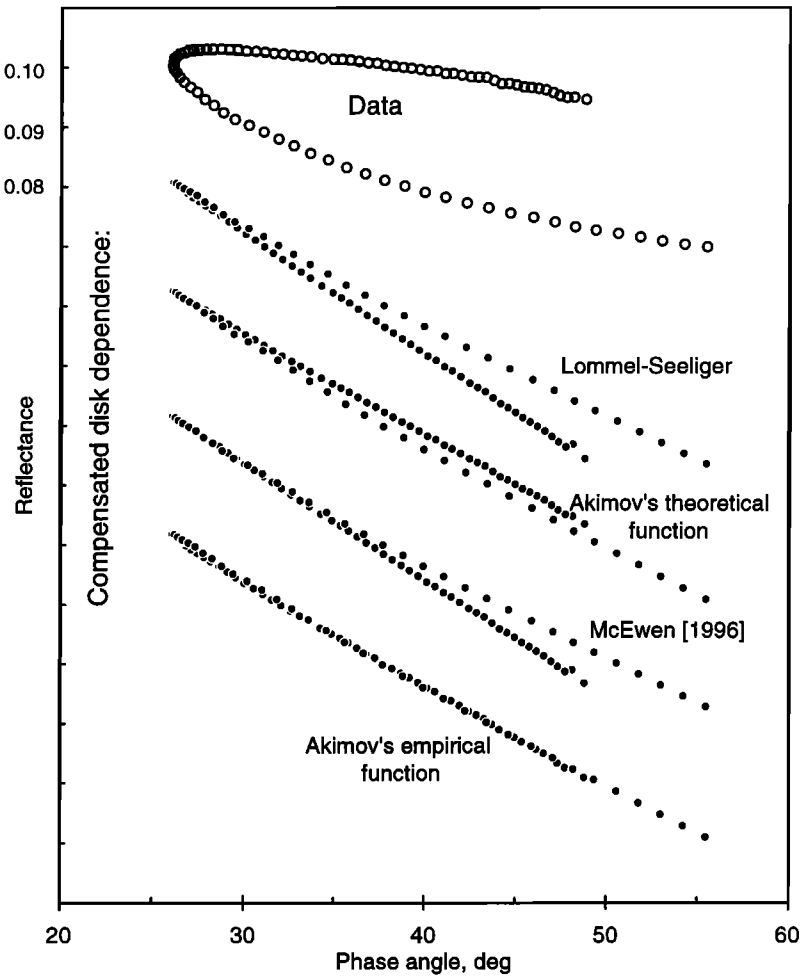

Figure 3. [DISKAKI.xls] The top curve represents average brightness of area 1 shown in Figure 1a for a sequence of frames from orbit 299 plotted against phase angle. The other curves represent the same values divided by different approximations of the disk function. Closeness of the two branches indicates good fit of the approximation used. The curves are arbitrarily shifted along the vertical axis. Approximations used, from top to bottom: Lommel-Seeliger law; McEwen's [1996] global disk function (17), (18); Akimov's [1988] theoretical function (21); and Akimov's [1988] empirical function (19), $\nu = 0.22$.

3.2. Approximations

Brightness changes along a single curve in the 3-D space of the angular parameters do not give complete information about the photometric function. Our aim is to study differences between the disk brightness distributions of different sites on the Moon. To describe these differences, we need an analytical approximation of the disk function. There are several theoretical functions to model observed brightness distributions [e.g., *Hapke*, 1993]. However, these functions are usually cumbersome and not convenient for data processing. In such cases, simple empirical or semiempirical functions are often used. For instance, *McEwen* [1991] suggested a convenient approximation in the form of a linear combination of the Lommel-Seeliger law ($D \propto \cos i / (\cos i + \cos \varepsilon)$) and the Lambert law ($D \propto \cos i$):

$$D \propto L(\alpha)\frac{2\cos i}{\cos i + \cos \varepsilon} + (1 - L(\alpha))\cos i\,. \qquad (17)$$

Here the balance factor $L(\alpha)$ decreases from 1 with increasing of α from 0. On the basis of Galileo images of the Moon, *McEwen* [1996] proposed the following polynomial approximation for $L(\alpha)$:

$$L(\alpha) = 1 + A\,\alpha + B\,\alpha^2 + C\,\alpha^3, \qquad (18)$$

where A, B, and C are the constant coefficients: $A = -1.9\times10^{-2}$, $B = 2.42\times10^{-4}$, $C = -1.46\times10^{-6}$.

Akimov [1979, 1988], on the basis of his astronomical measurements, proposed the following empirical expression to approximate the lunar disk function:

$$D(\alpha; b, l) \propto (\cos b)^{q(\alpha)}\,\frac{\left(\cos(l - \alpha/2)\right)^{q(\alpha)+1} - \left(\sin \alpha/2\right)^{q(\alpha)+1}}{\cos l}. \qquad (19)$$

Here parameter $q(\alpha)$ increases from 0 with increasing of α from 0.

Both functions (17) and (19) satisfy the reciprocity principle (12). Both functions predict uniform disk brightness at zero phase angle ($D(0; b, l) = \text{const}$). Both functions have the Lambert law as a limit case (for $L = 0$ and $q = 1$, respectively). Examples of dependences calculated with these formulae are shown in Figure 4.

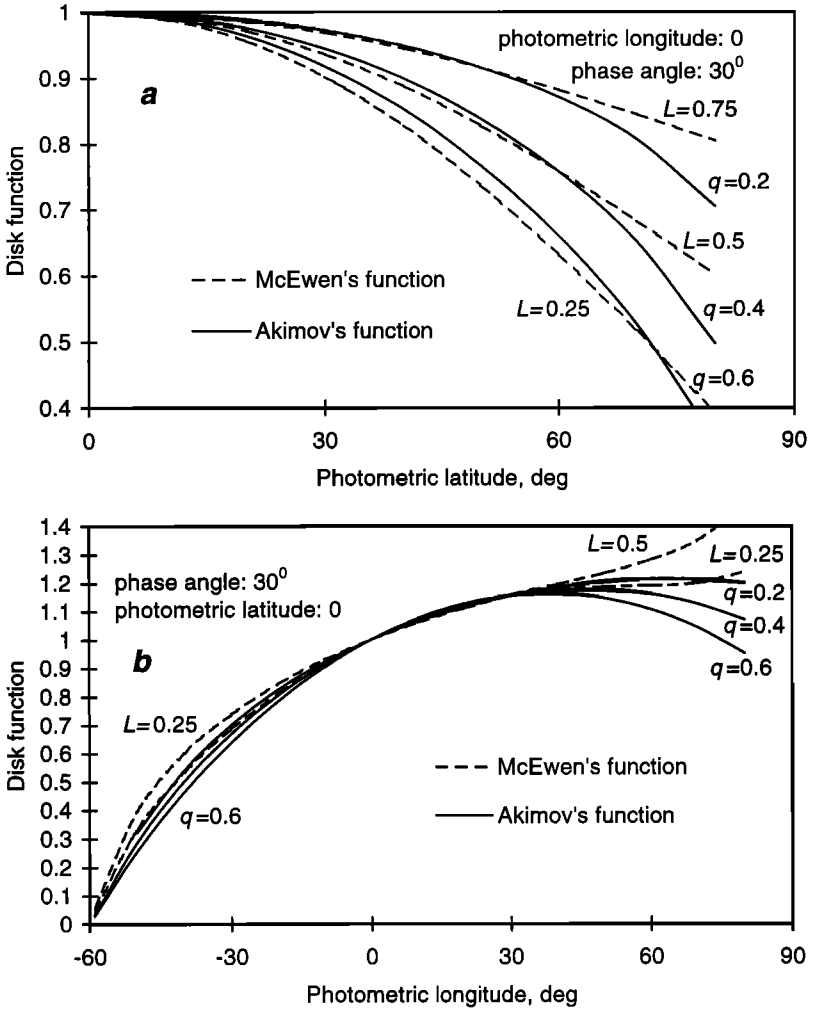

Figure 4. [CMPFNFIG.XLS] Comparison of empirical disk functions proposed by McEwen [1991] (equations (17) and (18)) (dashed lines, parameter L = 0.75, 0.5, 0.25) and by Akimov [1988] (equation (19)) (solid lines, parameter q = 0.2, 0.4, 0.6) for the phase angle $\alpha = 30°$. (a) Dependence on photometric latitude for zero photometric longitude (central meridian). (b) Dependence on photometric longitude for zero photometric latitude (photometric equator).

Equation (17) predicts limb brightening at moderate phase angles, which is not observed. In addition, the disk function (17) did not provide a perfect compensation of the disk brightness dependence for the studied sites at large phase angles (see an example in Figure 3).

Akimov [1988] found that for phase angles < 90° the dependence of q on α is linear: $q(\alpha) = \nu\,\alpha$, with $\nu = 0.16$ for maria and $\nu = 0.31$ for highlands. For this study we used (19) with linear $q(\alpha)$. Under normalization (14) this equation reads

$$D(\alpha;b,l) = (\cos b)^{\nu\alpha}\,\frac{\left(\cos(l-\alpha/2)\right)^{\nu\alpha+1} - \left(\sin\alpha/2\right)^{\nu\alpha+1}}{\left(\cos\alpha/2\right)^{\nu\alpha+1} - \left(\sin\alpha/2\right)^{\nu\alpha+1}}\,\frac{1}{\cos l}. \quad (20)$$

This function contains only one free parameter ν. By varying this parameter, we fit Clementine observations for all sites studied and all filters (Figure 3) to within the accuracy of measurements (1-2%). Thus we will proceed to examine variations of the disk function through variations of the only parameter ν. Values of ν providing the best compensation for all seven sites shown in Figure 1 are listed in Table 1. In Figure 5a these values are plotted against the wavelength.

Comparing the compensation with function (17) against that with function (19) in Figure 3, one needs to remember that in the former case the parameter set was chosen to fit the average disk dependence, while in the latter case the parameter was chosen to fit the test data themselves. We do not claim that function (19) provides a perfect disk function in the whole range of geometry and for any place on the Moon: Clementine data does not allow us to check this. However this expression does provide a reasonable approximation and is very convenient in this study.

It is worth mentioning one interesting theoretical expression for the disk function, which does not contain any free parameter. This is *Akimov*'s [1975, 1988] function:

$$D(\alpha;b,l) \propto (\cos b)^{\alpha/(\pi-\alpha)}\cos\left[\frac{\pi}{\pi-\alpha}(l-\alpha/2)\right]\frac{1}{\cos l}. \quad (21)$$

This disk function was derived from the formal condition that a surface being slightly randomly undulated should have the same disk function as before undulations [*Akimov*, 1975, 1988]. This disk function can also be derived for fractal-like surfaces [*Shkuratov et al.*, 1994; *Shkuratov*, 1995]. As noted by *Akimov*

Table 1. Parameter ν of the Disk Function (Equation (19)) and Parameter η of the Phase Function (Equation (21)) Derived From Series of Images for Areas Shown in Figure 1.

Wavelength, nm	ν	η
	Orbit 299 (Figure 1a) Area 1	
415	0.18	0 87
750	0.22	0.75
900	0.27	0 73
950	0.30	0.72
1000	0 33	0.72
	Orbit 299 (Figure 1a) Area 2	
415	0.15	0.82
750	0.22	0.72
900	0.26	0.70
950	0.29	0.70
1000	0.29	0.69
	Orbit 309 (Figure 1b) Area 1	
415	0.32	0.75
750	0.30	0.66
900	0.28	0.66
950	0.27	0.65
1000	0.28	0 66
	Orbit 309 (Figure 1b) Area 2	
415	0.35	0.71
750	0.32	0.63
900	0.32	0.64
950	0.31	0.64
1000	0.30	0.64
	Orbit 322 (Figure 1c) Area 1	
415	0.63	0.66
750	0.80	0.51
900	0.74	0 52
950	0.68	0.54
1000	0.78	0.50
	Orbit 322 (Figure 1c) Area 2	
415	0.57	0 67
750	0.74	0.52
900	0.69	0.52
950	0.67	0.53
1000	0.72	0.52
	Orbit 323 (Figure 1d)	
415	0.08	0 89
750	0.29	0.74
900	0.31	0.72
950	0.36	0.70
1000	0.44	0.67

[1979, 1988], (21) describes astronomically observed brightness distribution over lunar disk rather well, though somewhat worse than the empirical expression (19). The example in Figure 3 shows that the disk function (21) also provides a good compensation for the series of the Clementine images. When $\nu \approx 0.3$, function (19) is rather similar to (21) for moderate phase angles.

3.3. Regional Variations of the Disk Function

As seen in Table 1 and Figure 5a, values of ν vary widely, indicating that significant variations of the disk function occur. For the typical mare surfaces (orbits 299, 309, 323), ν varies from about 0.1 to 0.4, corresponding, for example, to a 0.65 - 0.45 range in the ratio $D(\alpha=60°; b=60°, l=0) / D(\alpha=60°; b=0, l=0)$.

The central part of the Reiner Gamma albedo feature (orbit 322) displays much higher values of the parameter ν. Estimation of ν in this series is less reliable, because data points on one of the branches are rather sparse (see Figure 2) and because the disk function (20) is less sensitive to variations of ν for higher ν. Note, however, that function (20) with $\nu < 0.4$ does not fit even our limited collection of observations of the Reiner Gamma formation. This means that the disk function for this site noticeably differs from that for typical mare surfaces. Probably, the enigmatic process, which produced increased albedo and spectral signature of immature regolith for Reiner Gamma formation [e.g., *Shkuratov et al.*, 1999b], has also strongly changed millimeter-decimeter-scale regolith structure. The Reiner Gamma disk function deviates from the "fractal" theoretical function (21) much more strongly than the disk functions for typical mare surface. The prominent "limb darkening" for the Reiner Gamma formation could imply a much smoother surface on the millimeter-decimeter scales than for typical lunar regolith surface [*Hapke*, 1984].

3.4. Disk Dependence of Color

Figure 5a shows that the spectral dependence of ν varies among typical mare sites, implying that color ratios depend on photometric latitude and longitude. Over the spectral range from blue to infrared light, the value of ν noticeably increases at the Apollo 15 landing site (orbit 299), more strongly increases in the vicinity of the crater Galilaei (orbit 323), and slightly decreases for Mare Cognitum (orbit 309). The spectral dependence of disk function means that color ratios can depend on the photometric latitude and longitude.

Examples of the observed changes in color ratios along the series are shown in Figure 6, where they are plotted against the phase angle. The color ratio is known to change with the phase angle: the lunar surface is generally redder at larger phase angles [e.g., *Mikhail*, 1970]. Lunar samples reveal the same behavior of color index [e.g., *Shkuratov et al.*, 1996]. Average dependence of the color ratio on the phase angle, obtained by *Shkuratov et al.* [1999a] from the Clementine data set, is also shown in Figure 6. It is clearly seen that the empirical color dependence differs from the average one and that the branches of the empirical color dependences are far from coincidence, especially for the Apollo 15 landing site. This is an observational demonstration of the existence of disk dependence of color.

If we believe that (20) describes the disk function accurately enough in a wide range of the photometric coordinates, we can predict how the color ratio would change under the constant phase angle. Such model calculations are presented in Figure 7 for the pair of ν of 0.1 and 0.3, which approximately corresponds to the blue/red difference in ν for the Apollo 15 landing site.

3.5. Phase Functions

The series of images of the same sites described above allowed us to compare the phase function of these particular sites. After the correction of the disk function, as described in section 3.2, we obtain the phase dependence of brightness (see Figure 3, bottom curve). To compare these dependences, we used an exponential approximation of the phase function:

$$f(\alpha) \propto \exp(-\eta\alpha)\cos\tfrac{\alpha}{2}\frac{(\cos\tfrac{\alpha}{2})^{\nu\alpha+1} - (\sin\tfrac{\alpha}{2})^{\nu\alpha+1}}{1-(\sin\tfrac{\alpha}{2})^{\nu\alpha+1}}. \qquad (22)$$

The cumbersome last multiplier in (22) came from the normalization (14). When parameter ν of the disk function (20) is known, the phase dependence of brightness is described by the only parameter η. Higher η means steeper phase function. This approximation of the phase function was used by *Akimov* [1979, 1988] in his study of the lunar phase function from Earth-based observa-

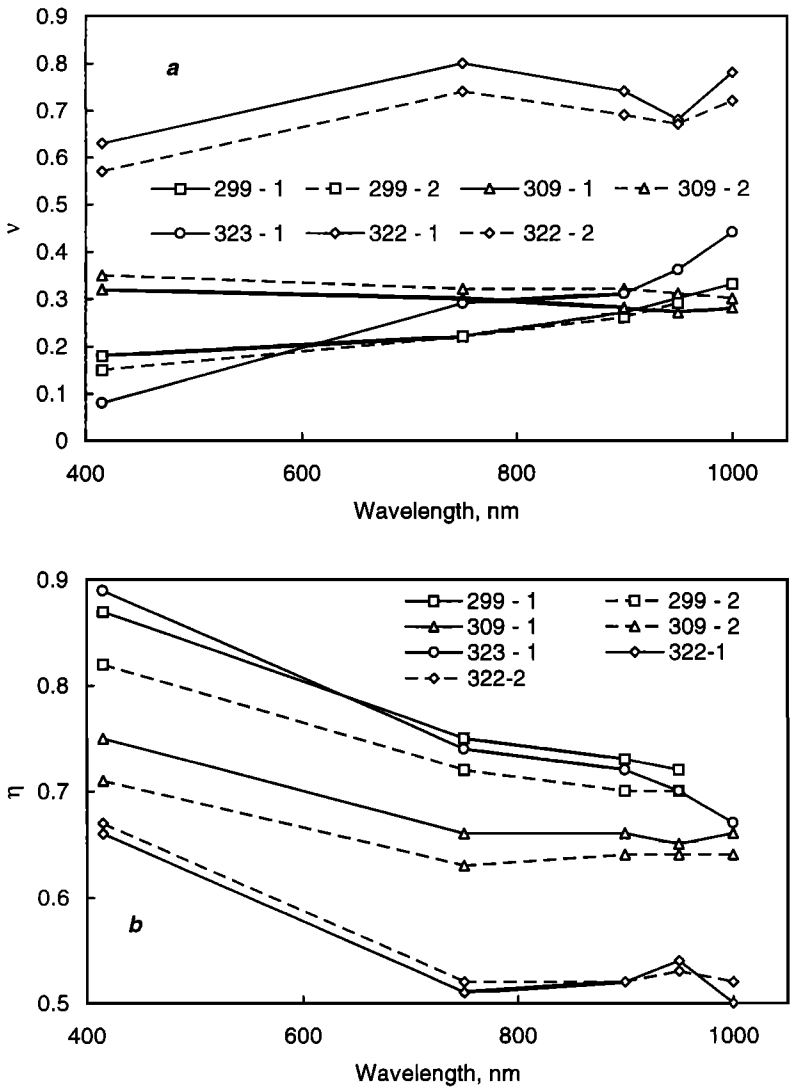

Figure 5. [COMPFNS.XLS->Velik. results] Wavelength dependence of (a) the parameter ν of the disk function (20) and (b) the parameter η of the phase function (22) for the seven sites listed in Table 1 and shown in Figure 1.

tions. For the range of the phase angles under consideration (25° - 60°) this approximation is rather close (though not identical) to the semiempirical phase function proposed by *Shkuratov et al.* [1999a]. The particular choice of approximation does not matter for this range of phase angles: the differences are essential for the small phase angles.

The results for all studied sites in the five filters are shown in Figure 5b. It is clearly seen that the phase function is steeper (η is higher) in the blue filter than in the red and infrared filters. This is the well-known reddening of the lunar surface with increasing of the phase angle.

It is also seen that there are systematic differences in η between the sites. In principle, the difference can be due to imperfection of the approximation (20) of the disk function. However, the paths in the space of *l*, *b*, and α are rather similar (though not the same) for all sites (Figure 2), and the loop (Figure 3) collapsed perfectly with the compensation of the disk dependence. This ensures that the difference in the obtained values of η reflects real difference in the phase function. For the Apollo 15 landing site the phase dependence of brightness is steeper in all filters than that for Mare Cognitum, though all the areas are rather typical mare surfaces. The Reiner Gamma formation has the least steep phase function< which, along with its peculiar disk function, implies that the surface is smoother than is typical for mare.

4. Opposition Effect

A number of UVVIS images contain zero phase angle points or, in other words, the spacecraft shadow points. These images allow us to study the peculiar behavior of the lunar phase function at extremely small phase angles [*Nozette et al.*, 1994; *Buratti et al.*, 1996; *Shkuratov et al.*, 1999a]. A similar approach based on image analysis has been used to investigate the opposition effect of the Moon during the *Apollo* missions [*Pohn et al.*, 1969, 1971], that of Mars with Viking data [*Thorpe*, 1982], and that of Jovian satellite Europa with Galileo data [*Helfenstein et al.*, 1998]. In this section we consider different methods to study the lunar opposition effect using Clementine image data. Preliminary results of this study for several sites were discussed by *Shkuratov et al.* [1999a]. Refinement of data analysis technique did not no-

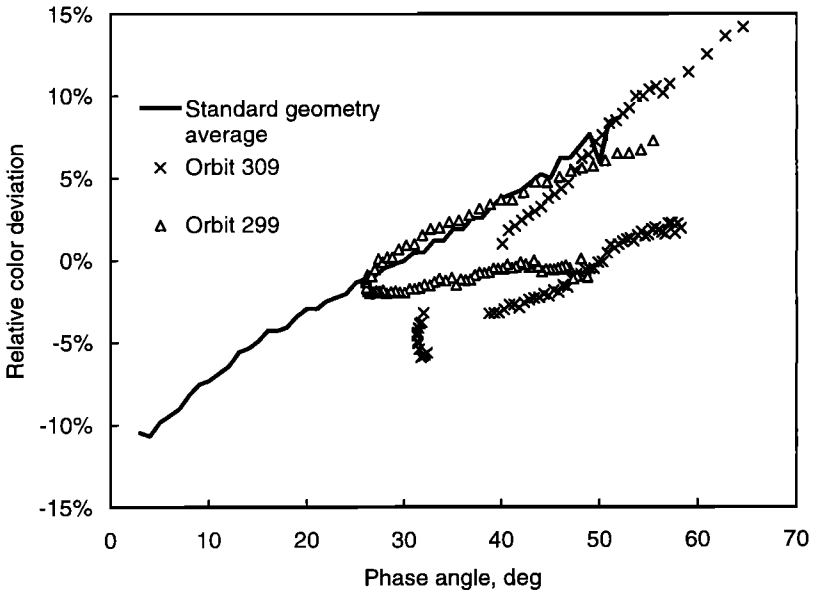

Figure 6. [DISLCOLO.XLS->Plot] Arbitrarily normalized color ratio 750 / 415 nm in the series of images for the sites shown in Figure 1a area 1 (triangles) and Figure 1d (crosses) plotted against the phase angle. The line represents arbitrarily normalized average phase dependence of the same color ratio at $b \approx l \approx 0$ derived from Clementine regular mapping data by *Shkuratov et al.* [1999a].

ticeably change the results presented and interpreted in that work. A greater number of studied sites allowed us to assess regional variations of the opposition spike.

4.1. Differential Method

The steepness of the lunar phase function sharply increases at small phase angles, forming the opposition brightness spike. This phenomenon is clearly seen in images as a diffuse bright spot around the zero phase angle point. An example is shown in Figure 8a. *Buratti et al.* [1996] studied the opposition spike through averaging of a number of UVVIS camera images. In this study we focus on examination of individual frames.

The problem is how to separate the opposition brightness variations from albedo details. To resolve this problem, we have proposed a differential method [*Shkuratov et al.*, 1997, 1999a; *Kreslavsky et al.*, 1998]. We chose all pairs of images taken in filters C (900 nm) and D (950 nm) with the spacecraft shadow point and coregistered images of each pair with accuracy of about 0.2 pixels. Then we calculated the C:D color ratio (see an example in Figure 8b) for these very close spectral channels. Variations of the color ratio are due to difference in the position of the spacecraft shadow point on the surface (caused by the spacecraft orbital motion) and due to variations of the regolith spectral properties. Differences in the phase functions in these very close filters are supposed to be negligible. The variations of the regolith spectral properties in this wavelength range are generally small. We excluded small areas of apparently peculiar intrinsic color ratios and/or atypical opposition spike (predominantly, small young craters and steep walls of large craters, that is, areas of presumably immature regolith; see Figure 8b). We neglected other intrinsic color variations and considered the ratio image as an image of a phase ratio distribution.

To obtain the phase function from the phase ratio distribution, we needed to know phase angles at each point of both source images. Camera-pointing data accompanying the Experimental Data Records are not accurate enough to calculate the angles directly. We found the center of antisymmetry of the ratio pattern to a precision of 1-2 pixels, thus deriving camera-pointing information directly from the image data. The center of antisymmetry is the center of the segment between the spacecraft shadow points in the pair of images. A shift of the point on the surface can be calculated from the spacecraft-positioning data accurately enough. Knowing this shift, we located the spacecraft shadow points. Knowing their positions, we calculated phase angles for each pixel for both coregistered images.

We made use of the fact that the phase angle difference for each point is small. Deviation of the ratio from the average color index divided by the phase angle difference is approximately equal to the logarithmic derivative of the phase function. We calculated the mean phase angle and the phase angle difference for each point. Examples of these distributions are presented in Figures 8c and 8d. We averaged the estimated logarithmic derivative for 0.1° wide phase angle bins and obtained the logarithmic derivative in the 0.2° – 2.1° phase angle range. The lower limit of this range is defined by the shift between the spacecraft shadow points; the upper limit is defined by the frame size. Examples of the obtained logarithmic derivatives of the phase function are shown in Figure 9. These examples cover all varieties of the results: missing curves are well inside the curve cloud shown in Figure 9. From the derivative it is easy to obtain the phase function with arbitrary normalization (see examples in Figure 10). All phase functions demonstrate sharp decreasing of the derivative at the phase angles below 0.3° (Figure 9). This decrease is due to the finite diameter of the solar disk [*Shkuratov*, 1991; *Shkuratov and Stankevich*, 1995].

4.2. Regional Variations of the Opposition Spike

Values of the derivative of the phase function at any phase angle vary from site to site by more than a factor of 2. This variation is wider for smaller phases. Thus the steepness of the phase func-

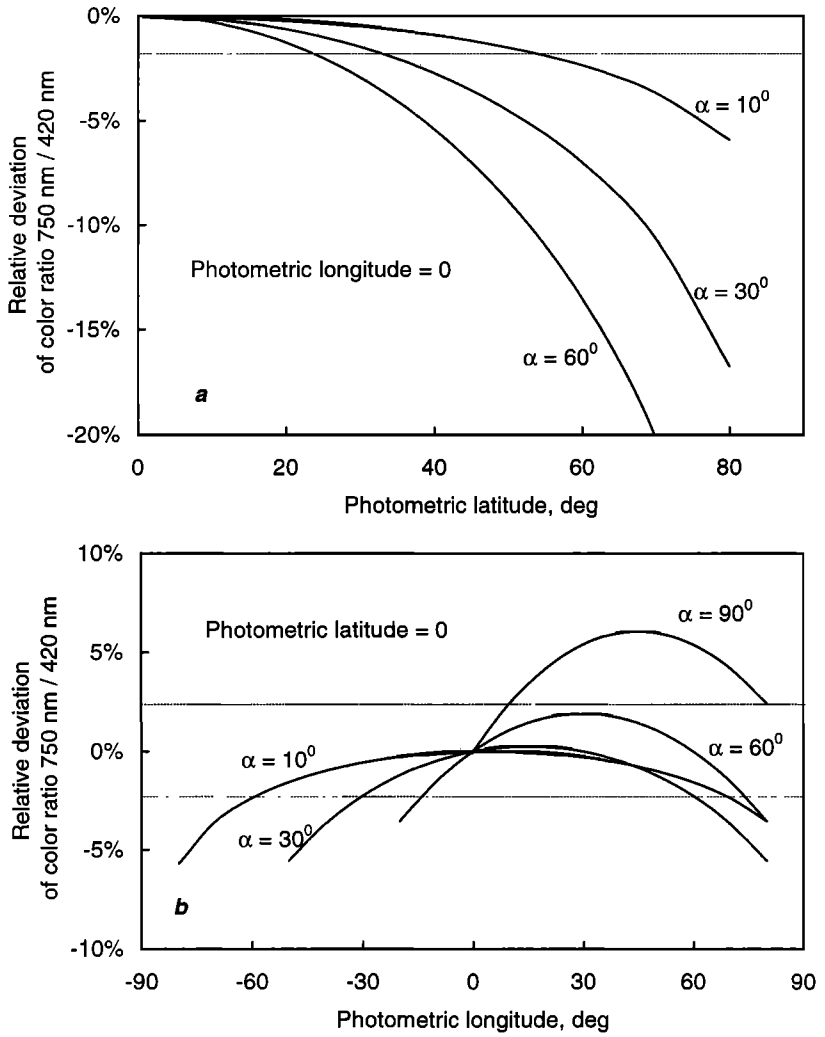

Figure 7. [COMPFNS.XLS->DiskColor] Approximation of the disk dependence of color calculated with function (19) for phase angles of 10°, 30°, 60°, and 90°. Calculations were done under the supposition that $\nu = 0.1$ for 420 nm wavelength and $\nu = 0.3$ for 750 nm wavelength. (a) Dependence on photometric latitude for zero photometric longitude (central meridian). (b) Dependence on photometric longitude for zero photometric latitude (photometric equator).

tion in the range of the spike is much more variable than that at larger phase angles. No definite dependence of the opposition spike on terrain type is observed. In Figure 11 the opposition spike amplitude in the 0.5°–1.5° range is plotted against reflectance. No well-expressed dependence of the opposition spike on albedo is seen. A weak trend of steepening the spike with increasing albedo could be recognized for the low-albedo part of the plot. At high albedos the spike tends to weaken with albedo increasing. A similar dependence of the opposition spike steepness on albedo had been noted for higher phase angles by *Shkuratov et al.* [1991] using telescopic observation of the Moon.

Although the amplitude of the opposition spike varies largely, the spike has a similar shape for all sites studied. In Figure 12 the spike steepness in the 0.5°–1° phase angle interval is compared with that in the 1°–2° interval. The values are highly correlated, demonstrating general similarity of the spike shape.

4.3. Direct Method

Another method that we applied to discriminate albedo variations and surface brightening due to the opposition spike is a direct method [*Kreslavsky et al.*, 1998]. For four of the 14 images with the spacecraft shadow point near the center, there are images taken at higher phase angles and covering the spacecraft shadow point. We coregistered the low-phase images and large-phase images or their mosaics. The large-phase images were taken at a phase angle of about 26°. Then we divided the low-phase image by the large-phase one. The albedo pattern is largely quenched, and the resulting image of the phase ratio can be used to study the opposition spike.

It is seen that besides the diffuse bright spot around the spacecraft shadow point, there is a pattern due to local topography variations in the phase ratio images. This influence of topography makes the method less precise compared to the differential method.

Another source of errors in this method is lower accuracy of the spacecraft shadow point location. As we noted above, the accompanied camera-pointing data are not accurate enough to locate the shadow point, but the spacecraft-positioning data are accurate enough to trace movement of the shadow point on the surface from frame to frame. We obtained the shadow point positions as the most probable centers of symmetry of the ratio im-

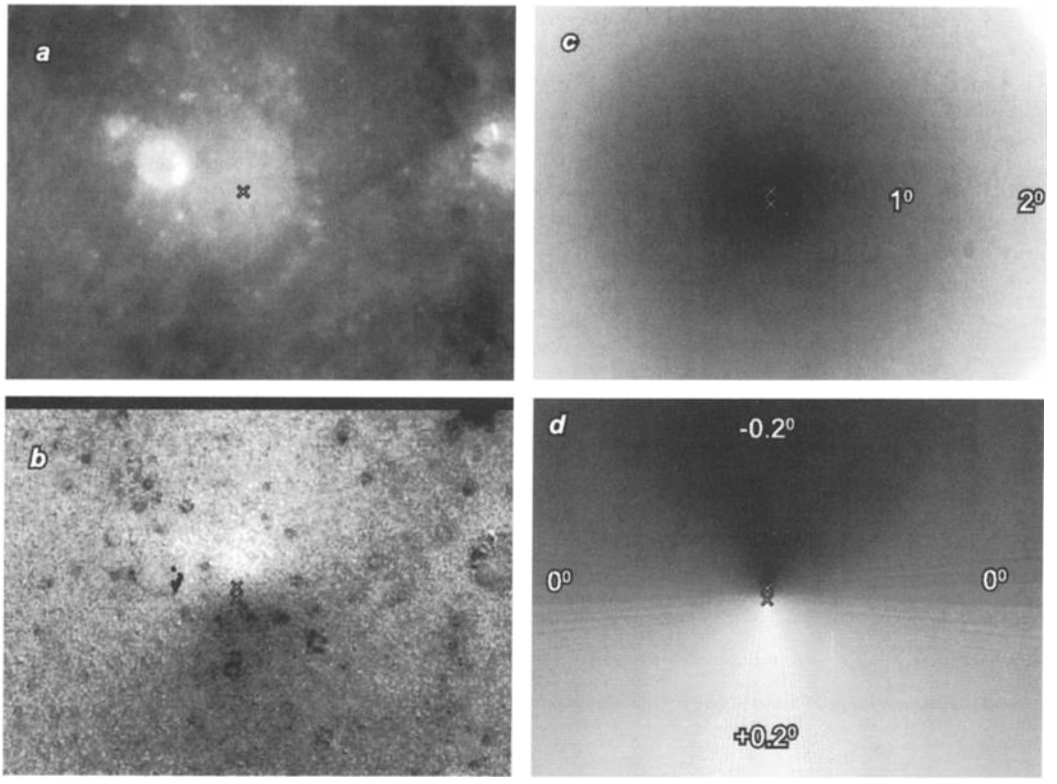

Figure 8. [DFFER.CV5] (a) The Clementine image LUC1974J.168 showing the opposition spot in the northeastern part of Sinus Medii; (b) the ratio of coregistered Clementine images LUC1974J.168 and LUD1970J.168; (c) distribution of the average phase angle; and (d) distribution of the phase angle difference. Crosses mark inferred positions of the zero phase angle points.

ages subject to the calculated shifts of the point between images in different filters. We checked the derived positions of the shadow points with that obtained with the differential method for the 900 nm filter.

We averaged the ratio values for a number of phase angle bins. This gave phase functions normalized to about 26°. Two examples of these phase functions are compared with those obtained for the same images with the differential method in Figure 10. A good agreement of the data obtained by different methods is seen. For the other two images this agreement is worse.

The images show some weak variations of the phase ratio, which are not apparently related to changes of phase angle and slopes. Probably, we observe some lateral heterogeneity of the phase ratio.

4.4. Spectral Dependence of the Opposition Spike

The advantage of the direct method is that it works for any filter. This allows study of the spectral dependence of the opposition spike parameters.

Figure 13 demonstrates a prominent dependence of the opposition surge on wavelengths. For instance, the phase ratio $I(1°)/I(26°)$ is greater at shorter wavelengths. The average phase dependences derived from Clementine data for the phase angle range 3°–50° show the same behavior [*Shkuratov et al.*, 1999a]. We saw the same behavior with the phase functions for the sites studied in section 3.5. This behavior of the phase function is well known from Earth-based observations.

For the area of Sinus Medii (Figure 13a) the behavior of the phase function at the smallest phase angles is very similar in all filters: the phase functions are equally steep. This is not the case for the vicinity of crater Godin (Figure 13b). Phase curves for this site are much noisier owing to observational errors caused by steep topography of the highland terrain. Data on the smallest phase angles (<0.2°), where statistics is poor, are not reliable. In the phase angles from 0.4°–0.7°, where statistics is better, the spike appears to be steeper for the shorter wavelengths.

5. Discussion

In this section we briefly discuss applications of our results to problems of photometric calibration of images of the Moon and another atmosphereless bodies.

5.1. Application to Clementine UVVIS Image Photometric Calibration

The gained knowledge of photometric properties of the lunar surface allowed us to estimate the relative accuracy of photometric calibration of images taken by Clementine with regular illumination/observation geometry. Photometric properties vary from site to site in a generally unmeasured way. These variations mean some inaccuracy in renormalizing of surface brightness or color ratio to the standard illumination/observation conditions.

Fortunately, regular imaging was done with $b \approx 0$, $l \approx 0$. That is why the revealed variability of disk dependence of brightness does not influence data too much.

Angular width of the UVVIS camera field is $4.2° \times 5.6°$, that is, about 7° along the diagonal. This means that the phase angle

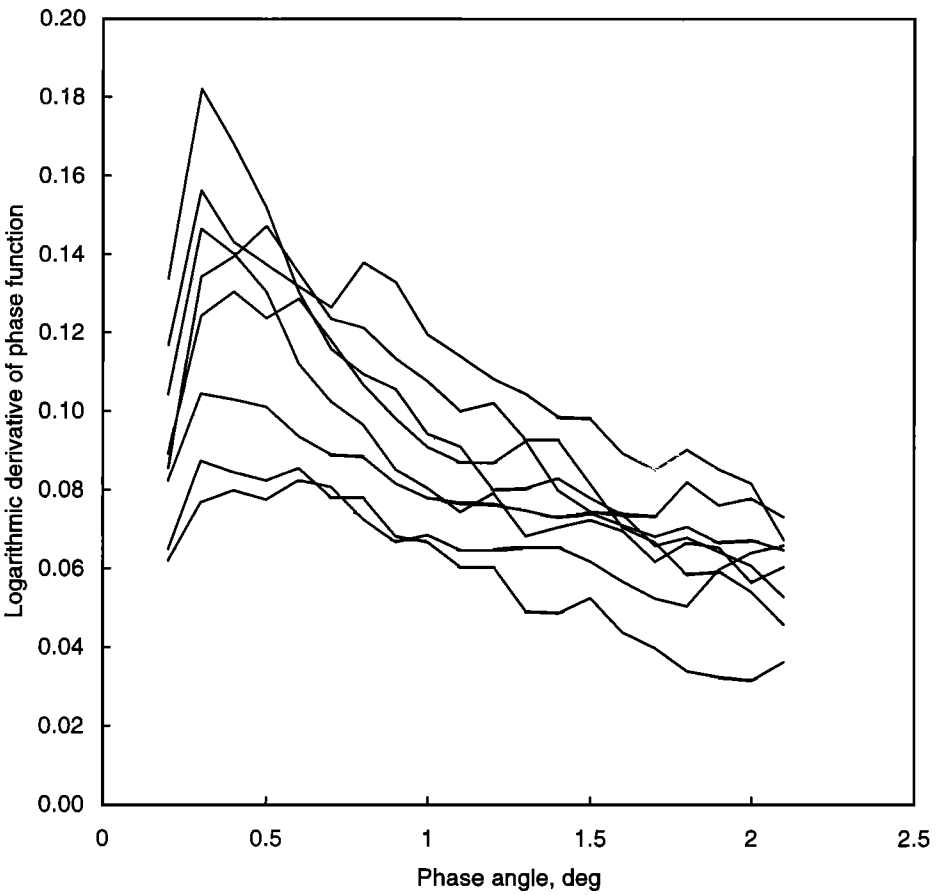

Figure 9. [DIFLGDER.XLS] Examples of logarithmic derivative of the phase function for the smallest phase angles obtained with the differential method.

α, photometric latitude b, and longitude l can change across the image in ranges from 4.2° to 7° wide.

Brightness changes due to change of b in such a range near $b \approx 0$ are negligible.

Brightness changes due to change of l can be ignored only for the smallest phase angles and should be corrected in a typical case. For example, at $\alpha = 30°$, a 7° change of l gives about 4% change in photometric function if we believe that the disk function is well described by function (19). The influence of the longitudinal dependence increases steeply with increasing of the phase angle. At large phase angles for the regular mapping the photometric longitude changes mostly along the short side of the frame. At $\alpha = 60°$ a 5° change of l gives about 15% change in the photometric function.

For the latter case the correction varies in the range of about 2% wide with changes of the parameter ν in expression (19) from 0.1 to 0.8. For smaller phase angles the range is narrower. This means that for $\alpha < 60°$, ignoring regional variations of the disk function does not give an error exceeding the measurement precision, and thus these regional variations can be ignored.

Regional variations of the phase function are more prominent and significantly influence the quality of the photometric calibration of the Clementine images. A detailed study of these variations is the matter of additional work and is not discussed here.

5.2. Application for Future Spectrophotometric Imaging of Atmosphereless Bodies

Images of planetary surfaces cannot be taken at the same illumination/observation geometry because of mission limitations. Knowing the photometric function, it is possible to adjust the measured spectra and normalize them to the same illumination/observation conditions. The accuracy of this photometric calibration depends on that how accurately the photometric functions are known. General similarity of the regolith small-scale structure formed by the micrometeorite impacts suggests general similarity of the photometric functions of such surfaces. On the other hand, our study of the Clementine data showed that the photometric function is slightly different for different areas of the lunar surface, even for the morphologically similar (mare) areas. For other planetary regoliths we should expect even wider variations. This means that the a priori knowledge of the photometric function is limited, and there is a principal limit for the accuracy of the photometric and spectral calibration of such data. However, careful planning of the observational conditions in the future missions can reduce the inevitable photometric inaccuracy.

There is a conventional wisdom that the best conditions for the spectrophotometric studies are high Sun (small incidence angle), high observer (small emission angle), and the phase angle larger

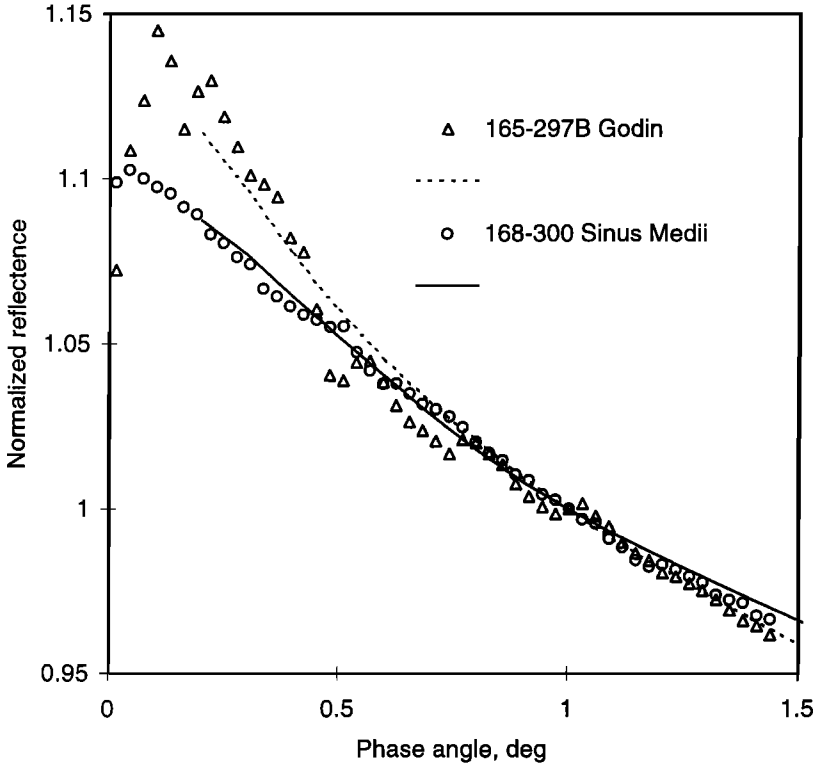

Figure 10. [TWOMETH.XLS] Examples of the phase functions obtained with the differential method (lines) and the direct method (symbols). The phase functions are normalized at 1°. The filter is 900 nm.

than the width of the opposition spike. Of course, our study confirms this general idea. We showed that the variations of the opposition spike are greater than variability of the photometric function at moderate phase angles. This means that studies of the opposition spike can contribute to knowledge about the surface structure and images taken at the smallest phase angles are interesting, but for studies of reflectance spectra such images should be avoided if possible.

Another lesson that we learned from our study of the Clementine images is the disk dependence of color and its variability. The approximation of the disk function that we used had been checked for the disk distribution of brightness seen from the Earth, and we showed that is matches the Clementine observations perfectly. This form of the disk function predicts that its variations are greater for greater phase angles. This implies that the use of rather small phase angles is preferable. For the phase angles lower than 20° the disk dependence of color does not ex-

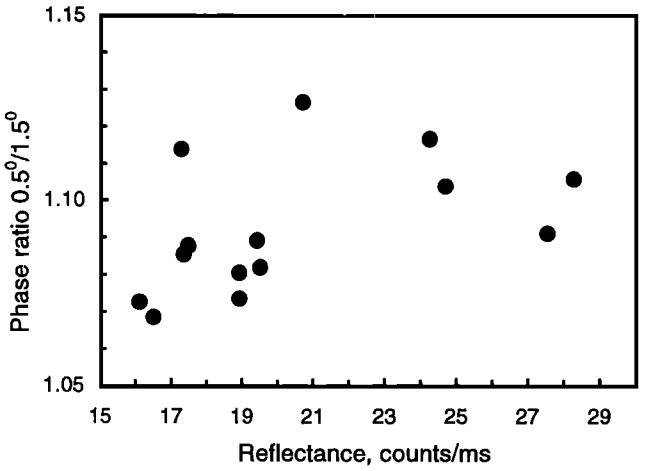

Figure 11. [DIFCORR.XLS] Phase ratio 1.5° / 0.5° obtained with the differential method for 14 pairs of images plotted against reflectance averaged over the area imaged under these phase angles. Reflectance is in arbitrary units (counts per millisecond).

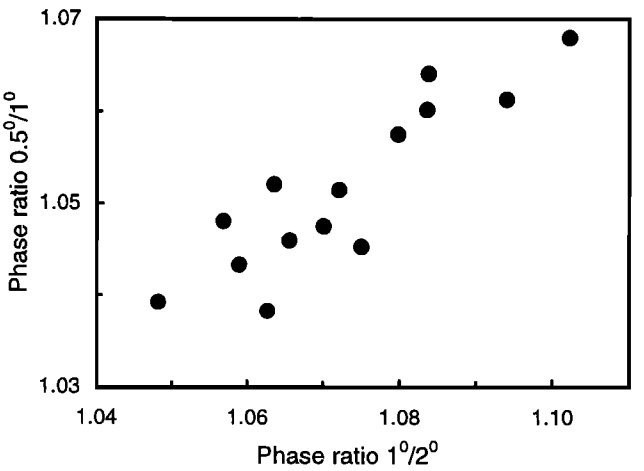

Figure 12. [DIFCORR.XLS] Phase ratio 0.5° / 1° plotted against phase ratio 1°/2°. Data were obtained with the differential method for 14 pairs of images.

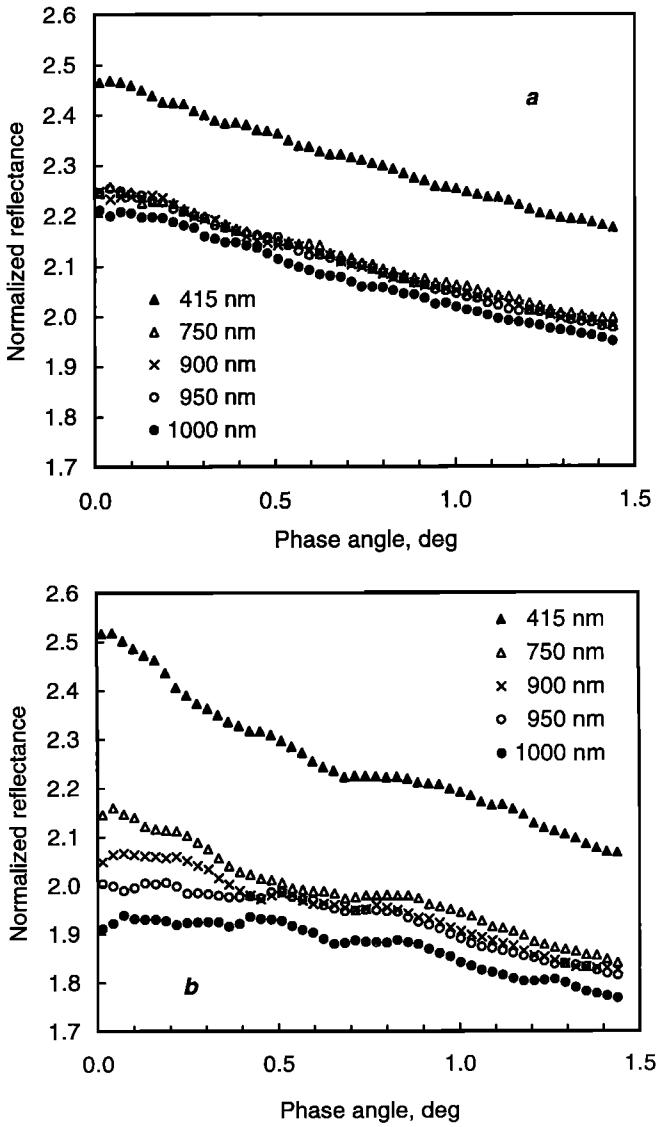

Figure 13. [RCTPLT.XLS->Plots] Phase functions derived by the direct method for the five filters. The functions are normalized at the phase angle of 26°. (a) Data derived from images from orbits 168 and 300 for an area in Sinus Medii. (b) Data derived from images from orbits 165 and 297 for a highland area and part of crater Godin.

ceed 1% and can be neglected, and the disk dependence of brightness can be compensated with the same accuracy up to incidence angles about 60°. Thus the best phase angles for the spectrophotometric measurements are in the range of about 10°–20°.

In particular, for the spectrophotometric study of the high-latitude regions of the Moon, where the Sun is low, better photometric calibration could be achieved for an oblique view providing smaller phase angles. Small phase angles are also preferable because at such observational conditions the influence of the surface slopes is much smaller. The latter is especially important for the future imaging of the asteroids because of their irregular shape.

6. Conclusions

Our study of the selected UVVIS image series from the Clementine data set led us to the following conclusions.

Short-term variations of the camera parameters limit potential relative photometric accuracy at the level of about 2%.

The disk function (that is, the dependence of the surface brightness on illumination/observation geometry under the constant phase angle) varies from site to site in the studied mare regions. There is a disk dependence of color, and this dependence also varies from site to site. These variations do not significantly reduce the accuracy of the Clementine spectrophotometry.

There is some evidence of differences in the phase dependence of brightness for different mare surfaces.

Reiner Gamma formation displays an unusual photometric function. This can be explained if the surface of this enigmatic albedo feature is smoother than typical mare regolith at small scales.

We found that the opposition spike varies from site to site. There is no obvious systematic dependence of the spike with albedo of the surface. Spectral dependence of the spike is also different for different sites. The spike parameters are controlled by small-scale surface structure, and their variability suggests that opposition spike measurements can be used to detect variations in regolith properties.

Acknowledgments. We would like to thank B. Hapke and P. Helfenstein for their extremely helpful comments on the manuscript. This study was partially supported by CRDF (grant UG2-295).

References

Akimov, L. A., The effect of mesorelief on the brightness distribution across the disk of a planet (in Russian), *Astron. Zh.*, *52*, 635-641, 1975.

Akimov, L. A., On the brightness distribution across the lunar disk and planets (in Russian), *Astron. Zh.*, *56*, 412-418, 1979.

Akimov, L. A., Reflection of light by the Moon. 1 (in Russian), *Kinematika Fiz. Nebesnykh Tel*, *4*, 3-10, 1988.

Buratti, B. J., J. K. Hiller, and M. Wang, The lunar opposition surge: Observation by Clementine, *Icarus*, *124*, 490-499, 1996.

Hapke, B., Bidirectional reflectance spectroscopy, 3, Correction for macroscopic roughness, *Icarus*, *59*, 41-59, 1984.

Hapke, B., *Theory of reflectance and emittance spectroscopy*, 455 pp., Cambridge Univ. Press, New York, 1993.

Helfenstein, P., et al., Galileo observations of Europa's opposition effect, *Icarus*, *135*, 41-63, 1998.

Kreslavsky, M. A., Yu. G. Shkuratov, and V. G. Kaydash, Lunar opposition surge observed by Clementine (abstract), *Lunar Planet. Sci., XXIX*, abstract 1118, 1998.

McEwen, A. S., Photometric functions for photoclinometry and other applications, *Icarus*, *92*, 298-311, 1991.

McEwen, A. S. A precise lunar photometric function (abstract), *Lunar Planet. Sci., XXVII*, 841-842, 1996.

McEwen, A., E. Eliason, P. Lucey, E. Malaret, C. Pieters, M. Robinson, and T. Sucharski, Summary of radiometric calibration and photometric normalization steps for the Clementine UVVIS images (abstract), *Lunar Planet. Sci., XXIX*, abstract 1466, 1998.

Mikhail, J. S., Color variations with phase of selected regions of the lunar surface, *Moon*, *2*, 167-201, 1970.

Nozette, S., et al., The Clementine mission to the Moon: Scientific overview, *Science*, *266*, 1835-1839, 1994.

Pieters, C. M. Lunar materials from the visible to mid-infrared: The effects of space weathering, *Int. Geol. Rev.*, *40*, 981-989, 1998.

Pohn, H. A., H. W. Radin, and R. L. Wildey, The Moon's photometric function near zero phase angle from Apollo 8 photography, *Astrophys. J.*, *157*, L193-L195, 1969.

Pohn, H. A., R. L. Wildey, and T W. Offield, Correlation of the zero-phase brightness surge (heiligenschein) with lunar-surface roughness, *Apollo 14 Prelim. Sci. Rep. Part F, NASA SP-272*, 1971.

Sayles, R. S., and T. R. Thomas, Surface topography as a nonstationary random process, *Nature, 271*, 431-434, 1978

Shkuratov, Yu. G., Estimating the effect of angular light source dimensions on the opposition brightness effect of atmosphereless bodies, *Sol. Syst. Res* , Engl. Transl., *25*, 54-57, 1991.

Shkuratov, Yu. G., Fractoids and photometry of solid surfaces of celestial bodies, *Sol. Syst. Res.*, Engl Transl , *29*, 421-432, 1995

Shkuratov, Yu. G., and M. A. Kreslavsky. A model of lunar photometric function (abstract), *Lunar Planet. Sci., XXIX*, abstract 1117, 1998

Shkuratov, Yu. G., and D G. Stankevich, Can lunar opposition spike measured by Clementine exist? (abstract), *Lunar Planet. Sci , XXVI*, 1295-1296, 1995.

Shkuratov, Yu., N. Opanasenko, A. Basilevsky, B. Zhukov, M. Kreslavsky, and S. Murchie, A possible interpretation of bright features on the surface of Phobos, *Planet Space Sci., 39*, 341–347, 1991.

Shkuratov, Yu., L. Starukhina, M. Kreslavsky, N. V. Opanasenko, D G Stankevich, and V. G. Shevchenko, Principle of perturbation invariance in photometry of atmosphereless celestial bodies, *Icarus, 109*, 168-190, 1994.

Shkuratov, Yu. G., L. Ya. Melkumova, N. V. Opanasenko, and D. G. Stankevich, Phase dependence of the color indices of solid surfaces of celestial bodies, *Sol. Syst. Res.*, Engl. Transl., *30*, 71-79, 1996.

Shkuratov, Yu G., M. A. Kreslavsky, and D. G. Stankevich, On the lunar opposition spike observed by Clementine New results (abstract), *Lunar Planet Sci , XXVIII*, 1307-1308, 1997.

Shkuratov, Yu. G., M. A Kreslavsky, A A. Ovcharenko, D. G. Stankevich, E S. Zubko, C. M Pieters, and G. Arnold, Opposition effect from Clementine data and mechanisms of backscatter, *Icarus, 141*, 132-155, 1999a

Shkuratov, Yu. G , V. G. Kaydash, and N. V. Opanasenko, Iron and titanium abundance and maturity degree distribution on the lunar nearside, *Icarus, 137*, 222-234, 1999b

Thorpe, T E., Martian surface properties indicated by the opposition effect, *Icarus, 49*, 398-415, 1982

Velikodsky, Yu., M. Kreslavsky, Yu. Shkuratov, L. Akimov, V. Korokhin, Analysis of Clementine data using an empirical photometric function (abstract), *Lunar Planet. Sci., XXX*, abstract 1039, 1999.

V. G. Kaydash, M A. Kreslavsky, Yu. G. Shkuratov, D G. Stankevich, and Yu. I. Velikodsky, Astronomical Observatory of Kharkov State University, 35 Sumska Street, Kharkov, 310022, Ukraine. (kreslavsky@mak. kharkov.ua)

C. M. Pieters, Department of Geological Sciences, Brown University, Providence, RI 02912.

(Received July 22, 1999; revised October 12, 1999,
accepted October 19, 1999.)